Utilizing Shallow Seismic Refraction, Electric Resistivity Tomography, And Ground Penetrating Radar Techniques, To Evaluate Geotechnical Properties At El Galala Plateau, Gulf of Suez, Egypt

Tarek F. Shazly [1] 🆔 **, Ahmed Abd. El Khafeef** [*2] 🆔 **, Salah sh. Saleh** [3] 🆔 **, Shokry A. Soliman** [4] 🆔 **,**

Mohammed H. Farag [5] 🆔

[1,2,3,4,5] *Laboratory of geophysics, Exploration department, Egyptian Petroleum Research Institute, Cairo, Egypt*.

Article information

Correspondence:
Name: Ahmed Abd. El Khafeef

Email: Gidaakh@hotmail.com

ABSTRACT

The current study is an attempt to identify possible subsurface structural features such as voids and cavities in the Galala area, Northwestern part of the Gulf of Suez, Egypt using shallow seismic refraction (SSR), electric resistivity tomography (ERT), and ground penetrating radar (GPR) data for assessment of the geotechnical seismic factors and their appropriateness to the local governing building code. For detecting voids & cavities features in subsurface rock, ERT and GPR are the best choices due to the high resistivity/dielectric contrast that exists between the fractures and cavities and the surrounding formation. Also, shallow seismic refraction (SSR) is used in foundation studies, civil engineering projects & geotechnical investigation (imaging the subsurface structure). The field measurements include six ERT profiles using Dipole-Dipole (DD) arrays measured across the expected fracture. Accordingly, two seismic profiles with different directions are done to detect the common fracture trends in the area. In addition, 7 GPR profiles are carried out for the detection of fracture and cavities. The combined results interpreted from the ERT and SSR records obtained over the suspected site in the study area could be divided lithologically into three zones. They are the main geological zones based on variation in resistivity and seismic velocities according to the competence of bed with slight thickness variation from one profile to another. The first zone is the upper layer of weathered limestone, gravel fragments, and fractured marl, which is distinguished by poor to somewhat fair rock quality. The zone is overlaid by the second zone, which has a lithology of fractured argillaceous limestone of intermediate quality. The third zone is the hardest layer because it contains the toughest layer of limestone and is distinguished by a high competent rock. The bedrock at the site has a velocity range is about 1652 to 1720 m/sec for S-wave and 2570 to 2640 m/sec with average 2605 m/sec for P-wave, which is related to very compact and hard limestone. All of the GPR profiles reflect the existence of cracks and discontinuity/weak zones, about 2-4 m from the surface level of the area, especially in the western part.

استخدام الانكسار الزلزالي الضحل، والتصوير المقطعي بالمقاومة الكهربائية، وتقنيات رادار اختراق الأرض، لتقييم الخصائص الجيوتقنية في هضبة الجلالة، خليج السويس، مصر

طارق شاذلى [1] ، **احمد الخفيف** [2]* ، **صلاح شبل** [3] ، **شكرى عبدالسميع** [4] ، **محمد فرج** [5]

[1,2,3,4,5] *معمل الجيوفيزياء, قسم الاستكشاف, معهد بحوث البترول المصرى, القاهرة, مصر.*

الملخص

تتضمن الدراسة الحالية تحديد الخصائص التركيبية تحت السطح مثل الفراغات والشقوق في منطقة الجلالة، الجزء الشمالي الغربي من خليج السويس، مصر باستخدام الانكسار الزلزالي الضحل (SSR)، وطريقة المقاومة الكهربية ثنائية الابعاد(ERT) ، والرادار المخترق للأرض (GPR). لتقييم الخصائص الجيوتقنية ومدى ملاءمتها لقانون البناء المحلي الحاكم. وللكشف عن الفراغات والتجاويف في الصخور تحت السطح، يعد ERT و GPR أفضل الخيارات بسبب التباين العالى فى المقاومة و العزل الكهربى الموجود بين الشقوق والتجاويف والتكوين المحيط. كما يتم استخدام الانكسار الزلزالي الضحل (SSR) في دراسات صخور الأساس ومشاريع الهندسة المدنية والدراسات الجيوتقنية (تصوير البنية تحت السطح).

وتشتمل القياسات الميدانية على ستة قطاعات كهربية ERT باستخدام تشكيل (Dipole Dipole) التي تم قياسها عبر الشقوق المتوقعة بالمنطقة. وبناءا عليها تم عمل قطاعين باستخدام الانكسار الزلزالي الضحل باتجاهات مختلفة لكشف اتجاهات الكسور الشائعة في المنطقة. بالإضافة إلى ذلك، تم تنفيذ 7 قطاعات ردار GPR للكشف عن الكسور والتجويفات. من خلال تفسير النتائج التى تم الحصول عليها من خلال هذه الطرق تم تصنيف التربة التحت سطحية في منطقة الدراسة من الناحية الطبقية إلى ثلاث نطاقات. وهي النطاقات الجيولوجية الرئيسية على أساس التباين في المقاومة الكهربية والسرعات الزلزالية حسب كفاءة الطبقة مع اختلاف طفيف في سمكها من مقطع إلى آخر. النطاق الأول وهو الطبقة العليا وهى عبارة عن طبقة من الحجر الجيري المتعرض للتجوية، وشظايا الحصى، وكسرات من المارل ، والتي تتميز بجودة صخرية رديئة إلى متوسطة إلى حد ما. النطاق الثانى والذى يمثل الطبقة الثانية والتي تحتوي على حجر جيري طيني متشقق ذو كفاءة وجودة متوسطة. الطبقة الثالثة وهي الطبقة الاكثر صلابة وتتمثل بطبقة من الحجر الجيري وتتميز بصخر عالي الكفاءة. تتراوح سرعة طبقة الاساس بالمنطقة من 1652 إلى 1720 م/ث لموجات القص (S-wave) و من 2570 إلى 2640 م/ث بمتوسط 2605 م/ث للموجات الافقية، والتي ترتبط بالحجر الجيري المضغوط والصلب. تعكس جميع مقاطع الرادار (GPR) وجود شقوق ومناطق انقطاع/ضعف على عمق حوالي 2-4 متر من السطح ، خاصة في الجزء الغربي للمنطقة.

Introduction

El-Galala plateau is one of the most promising regions for urban and tourists as well as industrial developments in Egypt. It houses the various activities, such as construction of tourist resort, residential area, King Abdullah University, and a new road linking Ain Sokhna to Zafarana. It's located at about 60 km south of Suez and to the southwest of Ain Sokhna in the northern part of the North Eastern Desert.

The study area overlooks the Gulf of Suez rising 600 m above sea level and it contains a large part of the backfill and fortifications, and bounded by latitudes 29°25'2.00" and 29°25'4.00"N and longitudes 32°24'34.00" and 32°24'34.40"E (Fig. 1). The area is capped by hard Eocene limestone beds that are characterized by karst and sinkhole features (CONOCO, 1987).
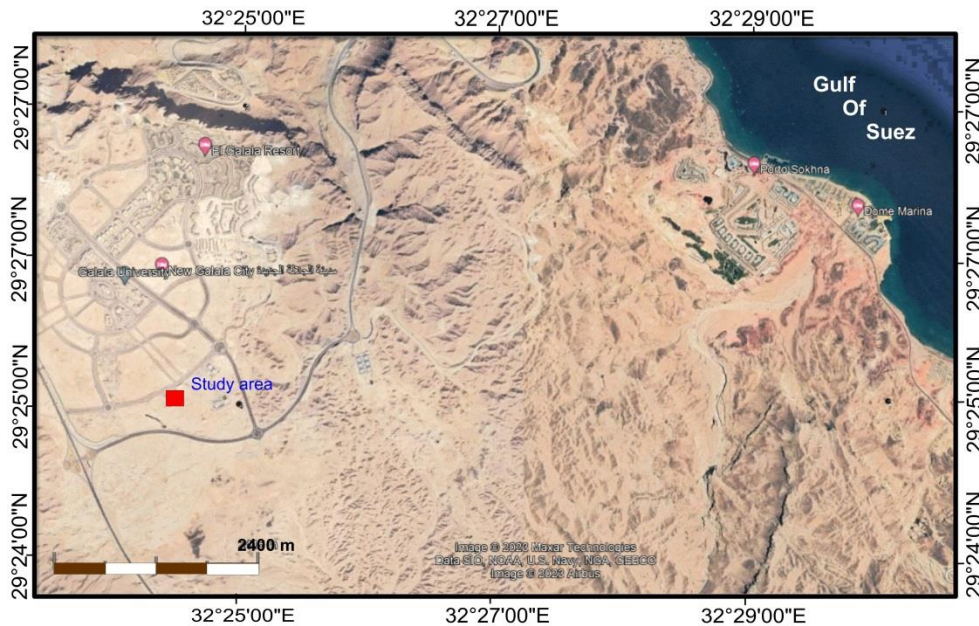
Fig. 1. Location Map of the Study Area

In the present work, results of ERT, SSR, and GPR methods are integrated to delineate the subsurface structures, fractures zones, expected cavities, sinkholes, voids, and cracks. Two seismic profiles were measured in the field in two separate orientations to begin identifying the prevalent fracture patterns in the region. Accordingly, six ERT, (DD) arrays were measured across the expected fracture strikes from seismic results. In addition, 7 GPR profiles were carried out to trace the fractures distributed over the whole region.

A geotechnical assessment is required prior to any suggested engineering design for construction to avoid a building collapse. Because each technique has a unique geophysical response with a different level of resolution, its integration into ground penetrating radar, shallow seismic refraction, and electric resistivity tomography techniques for site investigations is particularly successful. Geophysical investigations may be used in various geotechnical issues to determine the best course of action to reduce expenses, effort, time, and even the risk of accidents during any work. Effective geophysical techniques have been used in several studies to solve geotechnical problems including finding old building foundations, structure, cracks, and fractures saturated with water causing the subsidence for some parts of the constructions (Boudreault et al., 2010; Araffa et al., 2014), planning new cities, building new neighborhoods using the seismic velocity values to evaluate the competent rock quality of bedrock for the suggested construction region (Othman, 2005; Khalil and Hanafy, 2008; Silva, 2011). The reliable resistivity inversion results and seismic data are considered as a key role and a promising approach in studying the geotechnical parameters of the soil and rocks such as Atterberg limits unconfined compressive strength and bearing capacity (Attwa and El Shinawi, 2014; Eleraki et al., 2010, Shebl et al., 2019; Gemail et al., 2020; Baban et al., 2022). The capacity of the electrical resistivity imaging approach is selected to image the subsurface structure and layer thickness for this study. This method has several uses in engineering,

environmental studies and different subsurface explorations (Perrone et al., 2004; Loke, 2020). By this technique, the medium's apparent resistivity is measured. The relationship between the electrical current passing through the medium and the consequent potential difference can be used to calculate the apparent resistivity. A pair of electrodes, A and B, inject current into the ground, and two other electrodes, M and N, measure the resultant potential difference that results, both electrode pairs being fixed to the surface (Loke and Barker, 1992)

In the present study, the profiles were close to each other (Fig. 2). Most of these profiles were taken from the available places in the study area. The coordinates and elevations of all profiles are summarized in the Table (1).
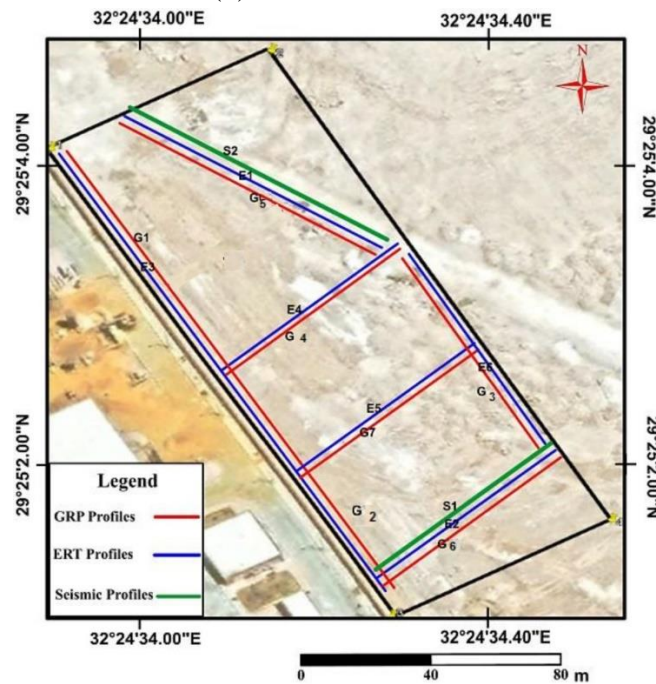
Fig. 2. locations of the acquired geophysical profiles in the Study Area

Geologic Setting

The stratigraphic succession beneath the study area began from the Precambrian complex of igneous and metamorphic rocks at the base, which is unconformably overlain by Phanerozoic rocks. The Phanerozoic sequence is composed mainly of siliciclastic-dominated rocks of Cambrian to Lower Cretaceous age and carbonate-dominated rocks of Upper Cretaceous to Eocene age.

Table 1: The coordinates and elevations of the studied profiles

Profiles	Coordinates (UTM)		Elevation (asl)	
	Start	End	Start	End
E1 S2 G5	442616.86 m E 3254456.34 m N	442666.97 m E 3254425.39 m N	545 m	543 m
E2, S1, and G6	442666.71 m E 3254342.72 m N	442704.56 m E 3254374.01 m N	536 m	537 m
E3, and G1,2	442600.69 m E 3254449.89 m N	442668.29 m E 3254338.35 m N	544 m	546 m
E4, and G4	442634.26 m E 3254395.38 m N	442670.92 m E 3254424.80 m N	544 m	542 m
E5, and G7	442650.77 m E 3254368.73 m N	442686.59 m E 3254398.33 m N	538 m	540 m
E6 G 3	442673.78 m E 3254423.96 m N	442702.21 m E 3254375.21 m N	542 m	537 m

E = Electrical resistivity profile S= Shallow seismic refraction profile and G = Ground penetrating radar profile

The carbonate rocks of the Middle Eocene Mokattam Formation, which unconformably overlies the Thebes Formation and has a discernible paleokarst surface, make up the majority of the highest portion of the Northern Galala (Farouk, 2015) (Fig. 3). The limestone strata that contain the distinctive *Nummulitesgizehensis* are a clear indicator of this formation. The principal diagenetic processes that affected the carbonate rocks of the Mokattam Formation, particularly along the main fault zone in the study area, include karstification, dolomitization, and dissolution. Karst landscapes, where bedrock erosion by water is one of the primary geomorphic processes, occupy 10%–20% of the land on Earth. Internal drainage, subsidence, and collapse caused by the growth of subterranean caves are mostly responsible for the genesis of the most significant surface karst features.

Methodology

Electrical Resistivity Tomography (ERT)

ERT Data Acquisition

Six profiles of two-dimensional electric resistivity tomography (2D-ERT) are carried out in the study area. In the ERT survey, dipole-dipole array is selected, which is the most sensitive to horizontal changes in the subsurface resistivities such in case of vertical structures like faults, fractured zones and cavities which are common in the surveyed area. The multi-electrodes resistivity meter (Syscal-pro 48, IRIS Corp., France) is used in the present investigation. Electrode spacing along the cables was 3 m with a total length of 69 m. An electric AC-current is transmitted into the ground through a pair of electrodes (current electrodes) and the resulting voltage difference is then measured through another pair of electrodes (potential electrodes).
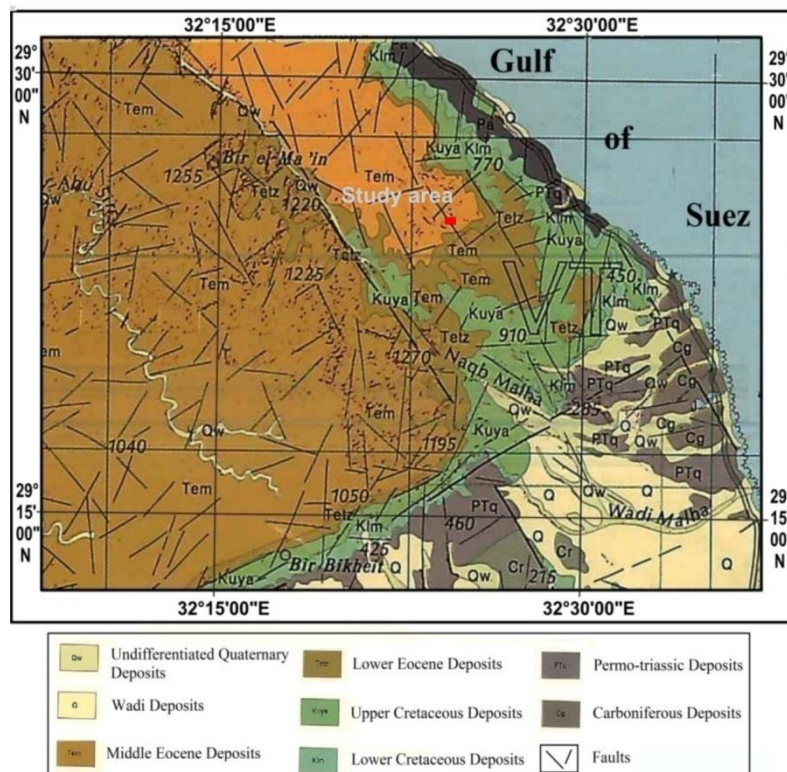
Fig. 3. Geologic map of the study area (CONOCO, 1987)

ERT Data Inversion and Data Interpretation

After the field survey, the resistance measurements are usually reduced to apparent resistivity values, converted into an interpretable resistivity model section (Shokry A. Soliman et al., 2020). The collected apparent resistivity raw data was dumped from the resistivity meter using special software. The data file was then introduced to processing 2D-resistivity tomography software "RES2DINV" version 4.10.3. Dealing with faulty data points is the first step in processing the apparent resistivity data. Before making a final assessment, such poor data points should be eliminated. The apparent resistivity readings are converted into genuine resistivity values using the commercial program RES2DINV. The inversion procedure is based on a quasi-Newton optimization method that implements smoothness constrained least-squares inversion. The results are displayed as pseudo-sections of apparent electric resistivity (Fig. 4A) that can be later inverted mathematically into electric resistivity-depth section (Fig. 4B) using 2D-modeling algorithms. This 2D-electric resistivity cross-section shows the lateral and vertical distributions in electrical resistivity that can be later interpreted to reveal the corresponding subsurface geologic cross-section.
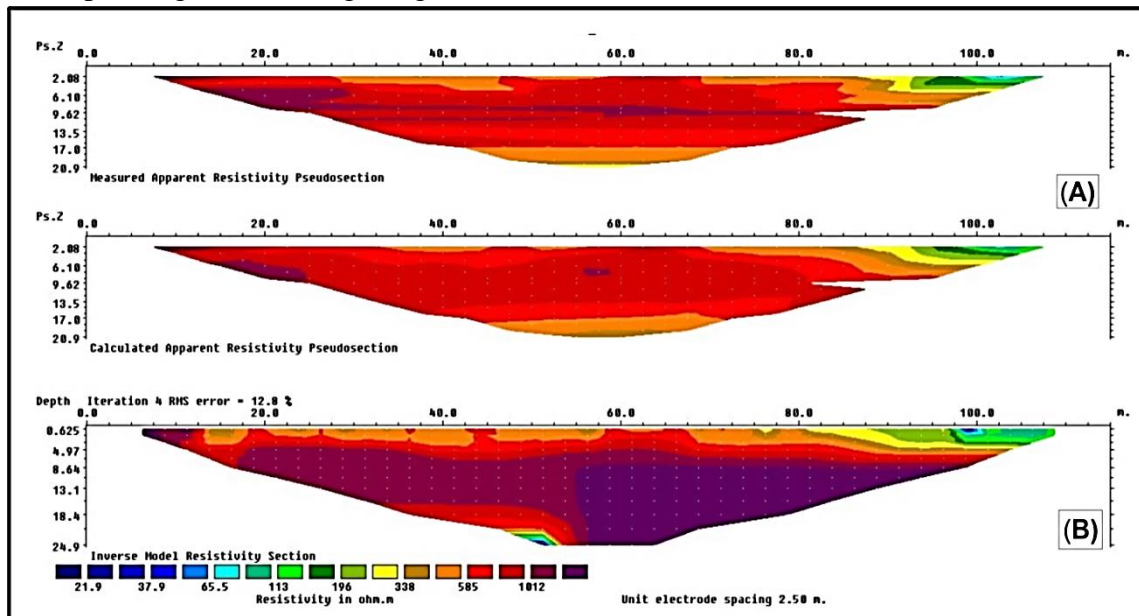
Fig. 4. An example of apparent resistivity pseudo-section (A) and the true resistivity cross-section (B).

The processing of data shows that all measured profiles (Fig. 5 to Fig. 10) reflect a displacement such as in profile E_1 and presence of fracture zone such as in profile E_2. These profiles consist of three layers which are the main geo-electrical zones according to variation in resistivity about (82-7750 Ohm.m) according to competent limestone with slight variation in thickness from one profile to another. The main three zones are described as follows:

The first zone is the top layer of weathered limestone, gravel particles, and fractured marl, which is characterized by poor to fair rock quality with resistivity readings under 1000 Ohm.m.

The second zone underlays the previous layer, its lithology is fracturing argillaceous limestone to moderate quality of competent rock with resistivity values range from 1000 to 2100 Ohm.m.

The <u>third zone</u>, which consists of compacted limestone used as bedrock, is the hardest layer and is distinguished by competent rock of high quality with resistivity values between 4200 and 7750 Ohm.m.

Shallow Seismic Refraction (SSR) Survey

Shallow Seismic Refraction Data Acquisition

The shallow seismic refraction profiling is carried out at a flat site in the investigated area. The collected data are used to estimate the P-wave and S-wave velocities to delineate the near-surface ground model beneath the investigated region.
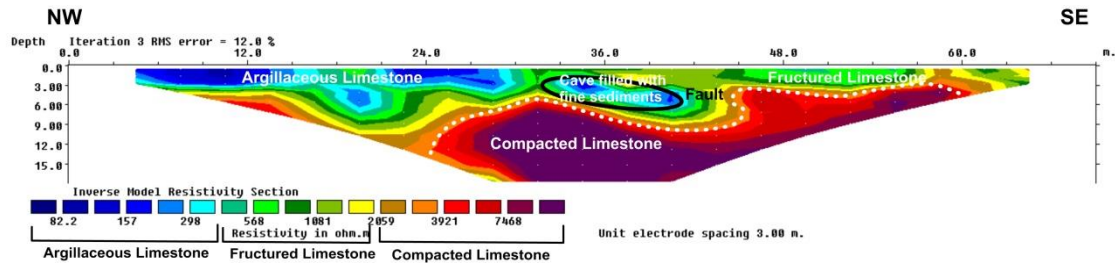
Fig. 5. The inverted ERT cross-section from profile No.1.
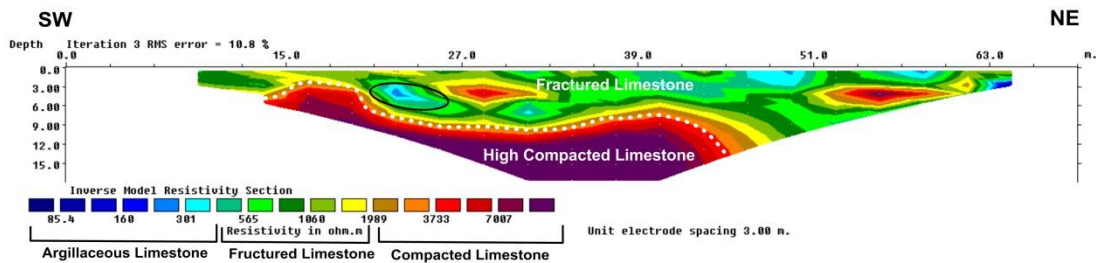
Fig. 6. The inverted ERT cross-section from profile No.2.
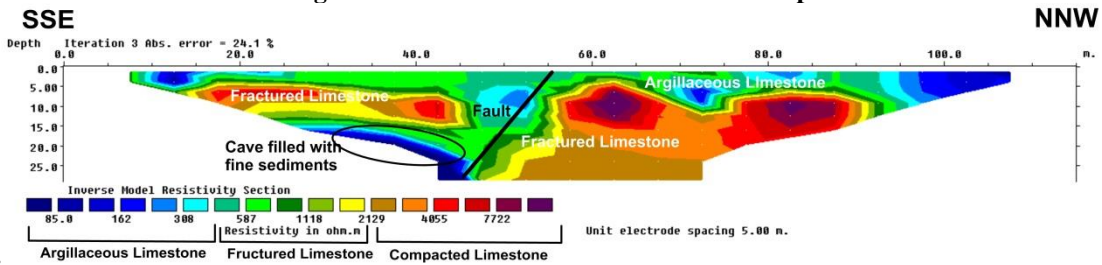
Fig. 7. The inverted ERT cross-section from profile No.3.
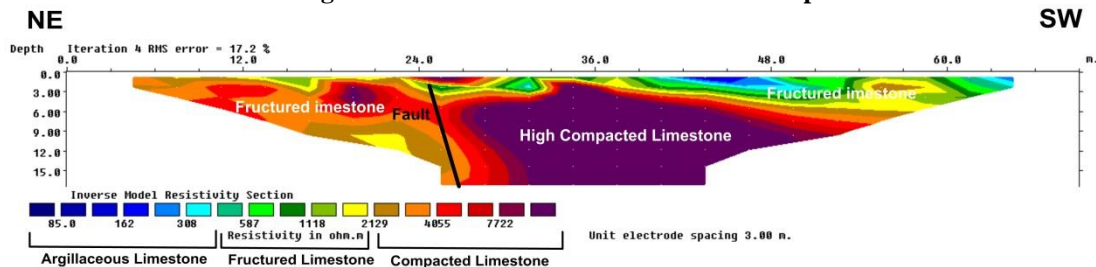
Fig. 8. The inverted ERT cross-section from profile No.4.
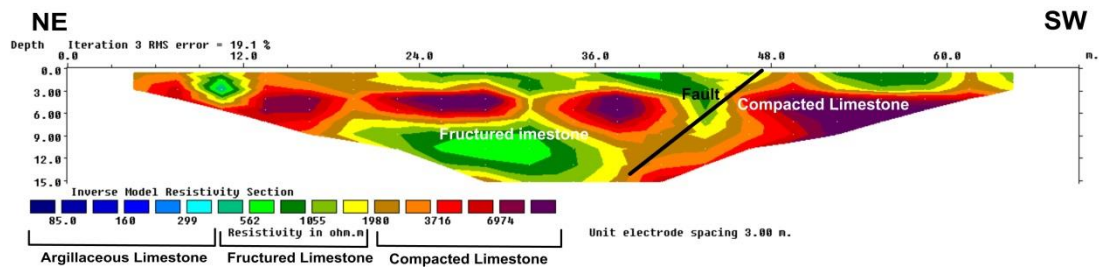
Fig. 9. The inverted ERT cross-section from profile No.5.
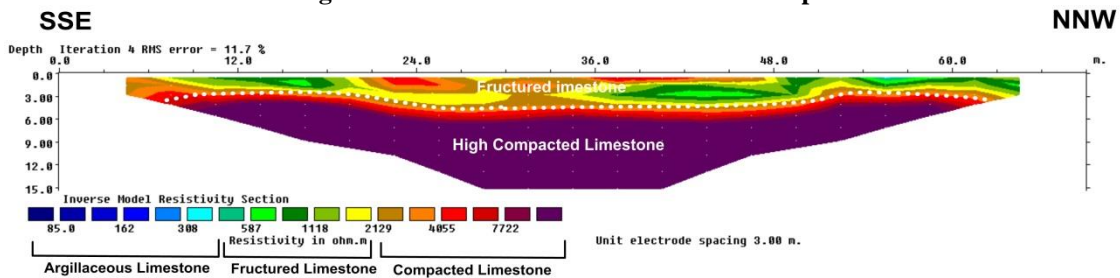
Fig. 10. The inverted ERT cross-section from profile No.6.

Several elastic moduli (Young's modulus, bulk modulus, shear modulus, compressibility and Poisson's ratio) and geotechnical parameters (concentration index, material index, stress ratio, ultimate and allowable bearing capacities) are extracted from the acquired data.

The foundation of the shallow seismic refraction approach is the ground-penetration of mechanical energy produced by an active seismic energy source like Sledgehammer. The 24 channel OYO MCSEIS-SX Seismograph's seismic recording equipment was used to collect the seismic data. Geophone spacing along the cables was 3 m; with a total length is 69 m. The resulting mechanical response is received, detected, amplified, and recorded by special equipment called seismograph and transforming into electrical energy as seismic signals (pulses), which are recorded by a special recording system. Using the time required for the wave to come back to the surface and the velocity of travel can determine the depth of different geological boundaries (Shokry A. Soliman et al., 2021).

Seismic Data Processing and Interpretation

The processing of the data is carried out to improve the data. The first step in the processing of the shallow seismic refraction data is to pick the first arrival times of the signal, called first break picking. The profiles were picked using the (Pickwin program version 4.2.0.0 of SeisImager software). A plot is then made showing the first arrival times against the distance between the shot and geophone. This is called a shooting record (Fig. 11). The picked data are interpreted using the ZONDST2D geophysical software version 5.1. to get the travel time - distance graph, then applying appropriate inversion techniques, which implies a systematic summation of arrival times from forward and reverse recordings shot.
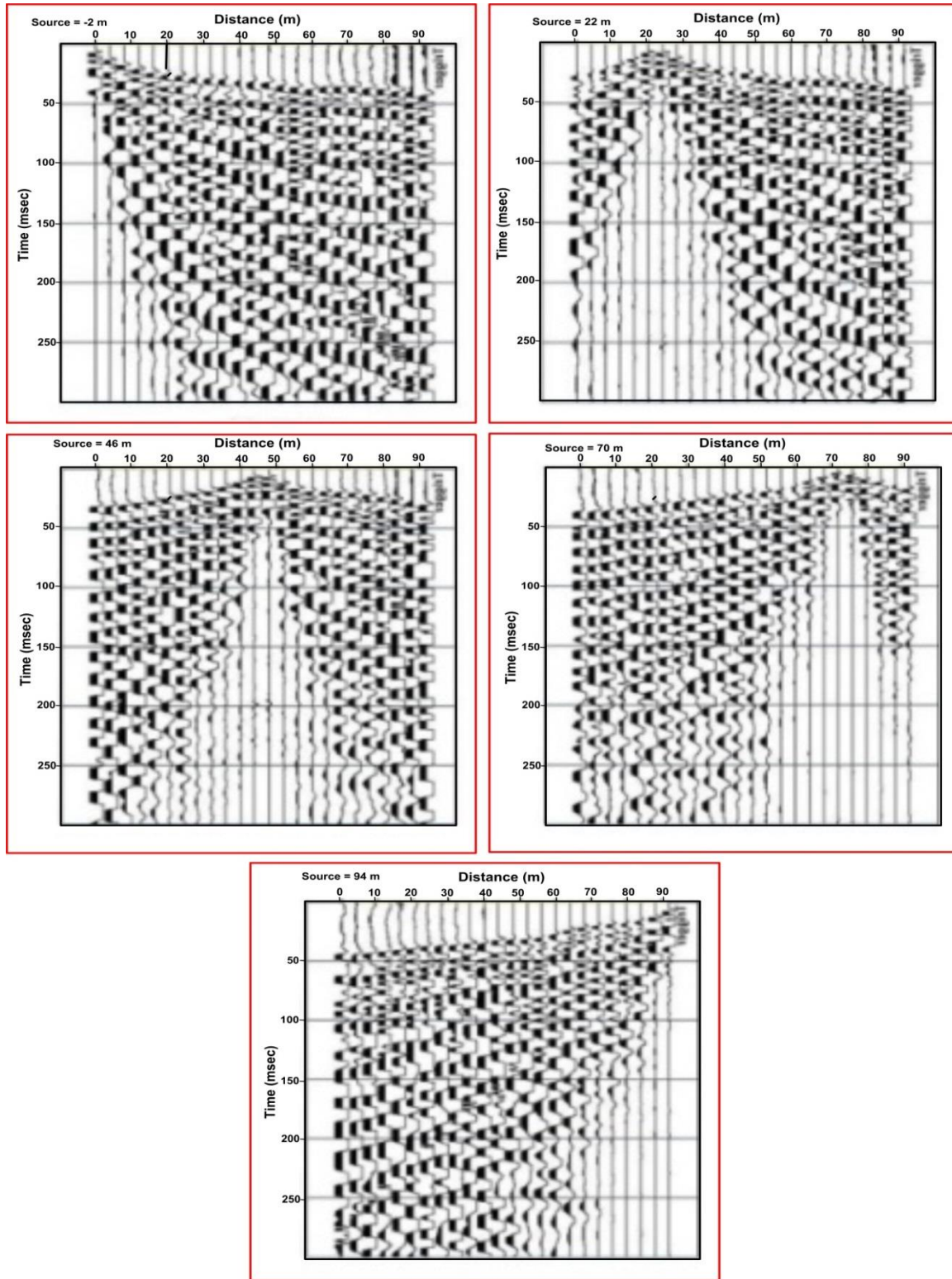
Fig. 11. The P-wave seismograms of the shallow seismic refraction survey of profile P1 as an example.

The depth and velocity of the subsurface layers are intended to be estimated through the interpretation of the seismic refraction data. To show the vertical and lateral distribution of each layer as well as the seismic profiles, the data are shown as depth-velocity models. The seismic profile (S_1) has mainly NE-SW direction explain fracture zones (Fig. 12). On the other hand, the seismic profile (S_2) is measured in nearly NW-SE direction across the trend of profile no.1, also it shows fracture zone and displacement (Fig. 13). The seismic velocities varied due to the

rock properties of the limestone bed. According to the seismic interpretation of all layered inversion velocity models, it is found that the compressional-wave velocity (Vp) values indicate the presence of three layers ranging from 590 to 644 m/sec with an average of 617 m/sec for the first layer (Vp1), 1516 to 1735 m/sec with an average 1625 m/sec for the second layer (Vp2), and finally 2570 to 2640 m/sec with average 2605 m/sec for the third layer (Vp3).The shear wave velocity (Vs) values of these three layers range from 347 to 378 m/sec with an average of 362 m/sec for the first layer (Vs1), 958 to 1027 m/sec with an average of 992 m/sec for the second layer (Vs2), and finally 1152 to 1230 m/sec with average 1191 m/sec for the third layer (Vs3).

Accordingly, it is noticed that the depth of penetration extends up to 15 m, and Geo-seismic models show three layers: The first layer has a thickness ranging from 1.5 m to 4 m can be considered as a surface layer of weathered limestone, fragments, and gravels. The second layer has a thickness ranging from 5.5 m to 12 m can be correlated as semi consolidated (layered) fractured argillaceous limestone. The third layer can be considered as compacted and hard layer of limestone.
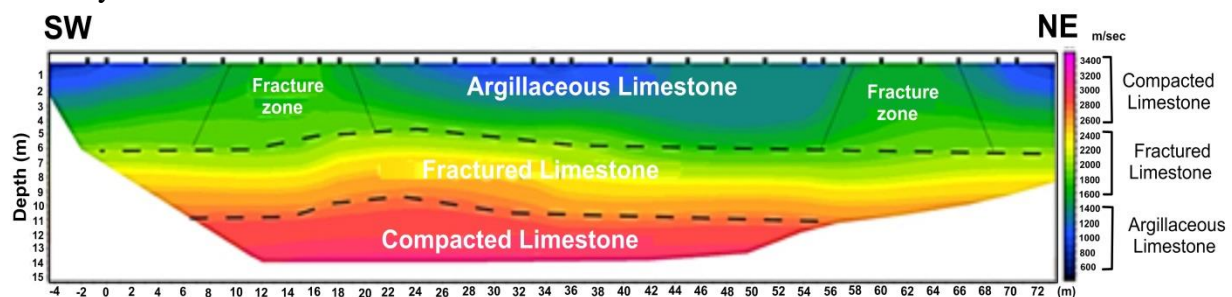
Fig. 12. The inverted SRT cross-section from profile No.1 (S1).
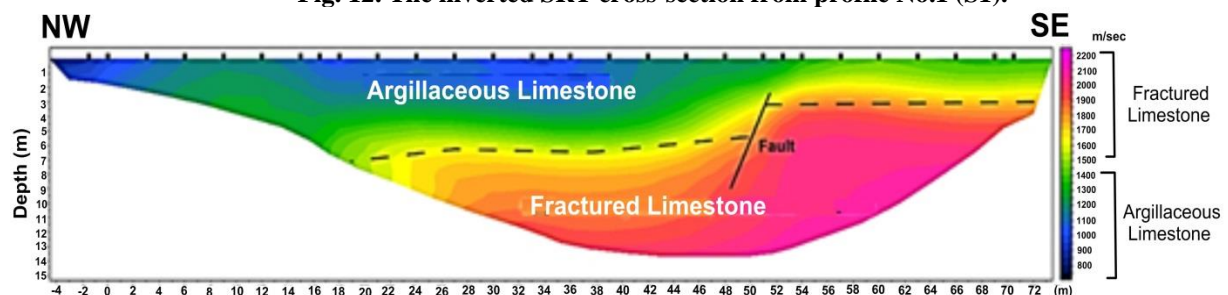
Fig. 13. The inverted SRT cross-section from profile No.2 (S2).

Geotechnical Parameters of the area

The Geotechnical parameters have been estimated for the soil material at the study area based on the compressional-wave velocities (Vp), shear-wave velocities (Vs), and bulk densities to provide direct information about its material quality. These geotechnical parameters are usually calculated for geotechnical and civil engineering purposes and for evaluating the competence and stiffness of the subsurface material (soil and/or rock) for construction, which contain more variables in engineering parameters than any other construction material (Table 4).

Table 2: Geophysical parameters of the conducted seismic layers

Layer No.	V_p	V_s	δ	ρ	μ	E	K	Ci	Mi	Si	Q_{ult}	Q_a
Layer1	644	378	0.273	1.56	202.4	515.2	377.8	4.67	-0.091	0.375	946.0	315.3
	590	347	0.251	1.53	176.6	442.0	296.3	4.98	-0.006	0.336	924.7	308.2
Layer2	1735	1027	0.230	2.00	2110.2	5192.5	3209.0	5.34	0.079	0.299	1335.2	445.1
	1516	958	0.218	1.93	1601.8	3903.2	2309.9	5.58	0.127	0.279	1290.3	430.1
Layer3	2640	1720	0.131	2.22	6573.8	14873.1	6722.0	8.62	0.475	0.151	1526.7	508.9
	2570	1652	0.148	2.21	6023.7	13829.6	6546.8	7.76	0.408	0.174	1511.8	503.9

where, V_p = P-wave velocity (m/sec), V_s = S-wave velocity (m/sec), δ = Poisson's ratio, ρ = density gm/cm^3, μ = Shear modulus (MPa), E = young's modulus (MPa), K = Bulk modulus (MPa), C_i = concentration index, M_i = material index, S_i = Stress ratio, Q_{ult} = ultimate bearing capacity (gm/Cm^2), and Q_a = allowable bearing capacity (gm/Cm^2).

The geotechnical parameters are calculated as follows:

1. Elastic moduli

a. Poisson's ratio (δ)

Poisson's ratio is calculated using the following equation (Sjogren, 1984):

$$\delta = \frac{[1-2(V_S^2/V_P^2)]}{[2-2(V_S^2/V_P^2)]}$$

Where; *Vp* and *Vs* are the compressional and shear wave velocities in m/sec respectively.

b. Rigidity modulus (μ)

The kinetic rigidity modulus (μ) is given in terms of shear wave velocity (V_S) and density (ρ) as follow:

$$\mu = \rho * V_s^2$$

Where; ρ: is the layer density in Kg/m^3, Vs: is the shear wave velocity in m/sec and, μ: is the shear modulus in Pascal.

c. Young's modulus (E)

Young's modulus (E) is given in terms of rigidity modulus (μ) and Poisson's ratio (δ) as follows:

$$E = 2\mu\,(1+\delta)$$

d. Bulk modulus (K)

The bulk modulus (K) is given in terms of Young's modulus (E) and Poisson's ratio (δ) as follow:

$$K = \frac{E}{3(1-2\delta)}$$

2. Competence scales

a. Material index (M_i)

The material index is given by the elastic modulus (Abd El-Rahman, 1989) as follows:

$$M_i = (1 - 4\delta)$$

Where: δ is Poisson's ratio.

b. Concentration index (C_i)

The concentration index can be given in terms of velocity squared ratio (Birch, 1966) as:

$$C_i = \frac{(3 - 4\propto)}{(1 - 2\propto)}$$

Where: α is the velocity squared ratio = (V_s^2/V_p^2).

c. Stress ratio (S_i)

The Stress ratio (S_i) was given by (Thomson, 1982) as:

$$S_i = \frac{\delta}{(1 - \delta)}$$

3. Foundation bearing capacities.

a. Ultimate Bearing Capacity (Q_{ult})

The ultimate bearing capacity in gm/cm^2 can be given in terms of shear wave velocity (Parry, 1977) as follows:

Log Q_{ult} = 2.932(logV_s–1.45)

b. Allowable Bearing Capacity (Q_a)

According to Parry, 1977), the allowable bearing capacity (Q_a) can be calculated as follows:

Q_a = Q_{ult} / F

Where Q_a is the allowable bearing capacity and F is the factor of safety equals three for cohesive soils.

Ground Penetrating Radar Survey (GPR)

GPR is an electromagnetic geophysical method used to acquire information about subsurface materials (according to ASTM D6432-99) based on high-frequency (25 MHz–3 GHz) electromagnetic wave propagation. In the present work, the ground penetrating radar "GPR" survey is conducted to detect the underlying features such as cavities/voids and fracture zones. The survey is carried out using the MALA GPR system with the ProEx control unit. The system is connected to the 100 MHz MALA shielded antenna. The GPR survey is carried out along the study area to detect subsurface cracks, cavities, anomalies, and weak zones. The diffraction signatures of the cracks, joints, fracture zone, voids, and caves are reviewed and recognized.

FIELD PROGRAM AND SURVEY

The data are displayed using a laptop computer, and the survey operations with 100 MHz antennas used in the present study. The system is powered by a 12V battery, the transmitting antenna is plated directly to the ground, and wheel calibration was made along 10 m in the distance, velocity used in calibration 120 m/ns and No. of stacking equal to 16. Seven GPR profiles were performed in the study area which is distributed in the available places (Fig. 2). The lengths of GPR profiles range from 20 m to 150 m. The device was set to acquire 310 ns as a target range, which in turn could reach more than 18 meters beneath the ground surface and a point interval of 0.025 m. The acquired data are subjected to processing, then interpreted in structural features Fig (14).
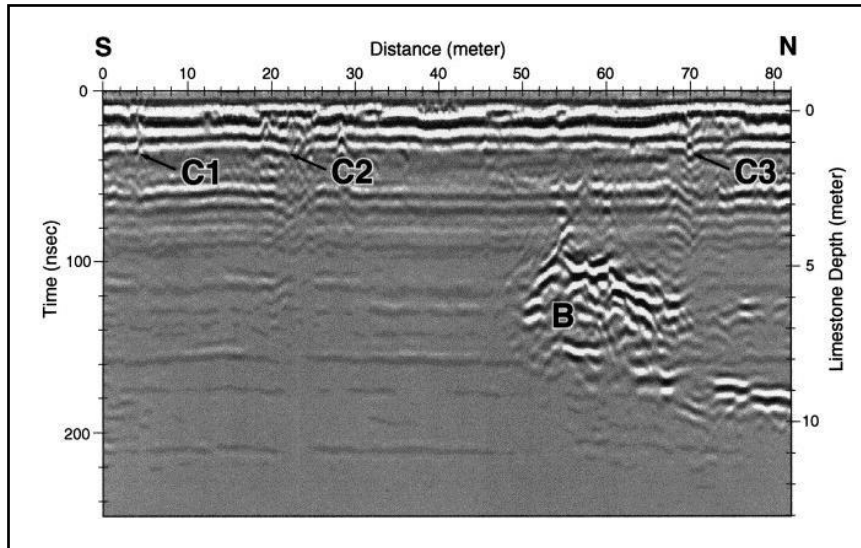
Fig. 14. A reference GPR profile shows the diffraction signatures of both the cracks (C) and the cave (B) within rocks (FitzGerald et al., 2001).

DATA PROCESSING AND INTERPRETATION

The post-processing sequences applied to the data set different from one segment measurement to another depending on the underground surface content and the surface pass of the profile. However, some processing steps are common such as moving the start time to adjust the zero time, applying background removal, applying the gain to enhance the desired low signals and wave velocity of 0.12 m/ns was used to convert the two ways travel time of the signal into depth in meter based on the electromagnetic wave velocity in limestone (Table 5).

In order to interpret fully the acquired GPR profiles along the study area, an intensive geophysical review was carried out to understand and knowing the diffraction signatures of the underground caves and cracks. From Figs. (12&13), the cracks and fracture zones shows discontinuity for the horizontal bedding of the subsurface layers. On the other hand, limestone caves show ringing in the radar diffraction, and such radar ringing is considered as a signature for any cavity that exists in the subsurface materials.

Accordingly, when the interpretation of the measured data in the Galala area is accomplished, we found that all of the GPR profiles reflect the existence of cracks and discontinuity/weak zones, about 2-4 m from the surface level of the area, especially in the western part along the wall of the water station, and also in the eastern part along the edge of the mountain. Furthermore, some profiles delineate the presence of a cavity and voids filled with sediments. The following figures reveal each GPR profile with the interpreted features and brief comments (Figs. 15 to 21). The locations of the cavities/voids and fractured-filled sediments are summarized in Table (6).

Table 3: Typical dielectric constant, velocity, electrical conductivity, and attenuation values of common subsurface materials (Leckebusch, 2003).

Material	Dielectric Constant	Electrical Conductivity (mSm^{-1})	Velocity (m ns^{-1})	Attenuation (dB m^{-1})
Air	1	0	0.3	0
Saltwater	80	3000	0.033	600
Fresh water	80	0.5	0.033	0.1
Ice•	3-4	0.01	0.18	0.01
Basalt. wet	5	0.01	0.11	0.01
Limestone•	4-8	0.5-2	0.12	0.4- 1
Shales*	5-15	1-100	0.09	1-100
Sand, dry	5	0.01	0.13	0.01
Sand, wet	20-30	0.1·1.0	0.06	0.03-0.3
Clay, wet	10	500	0.095	300
Soils:				
sandy, dry	3	1.4	0.19	1
sandy, wet	25	69	0.06	23
Clayey, dry	3	2.7	0.19	3
Clayey, wet	19	500	0.07	200
frozen	6	0.1	0.12	0.1
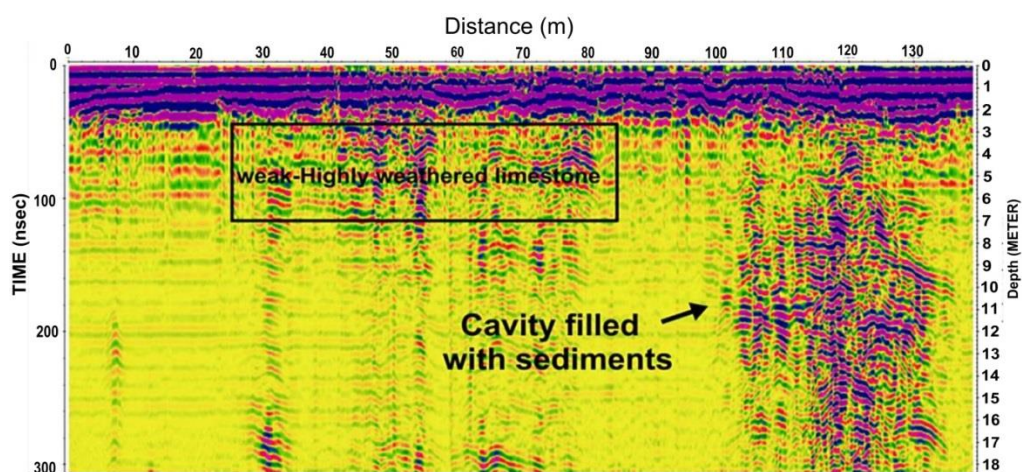
Fig. 15. The inverted GPR profile No. 1
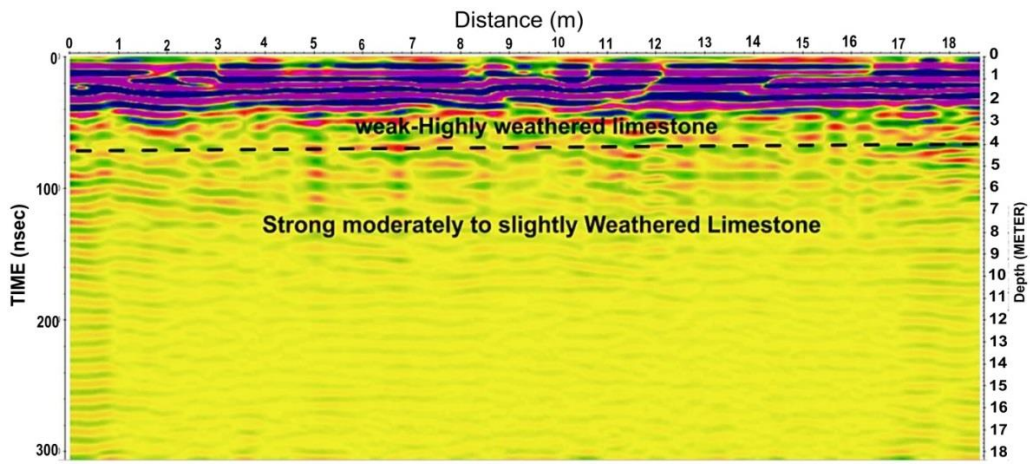
Fig. 16. The inverted GPR profile No. 2
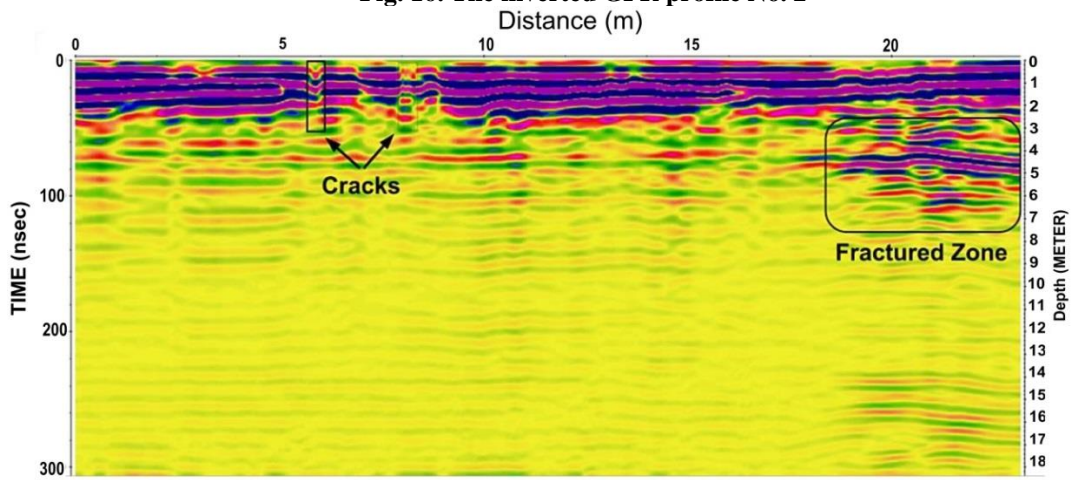
Fig. 17. The inverted GPR profile No. 3
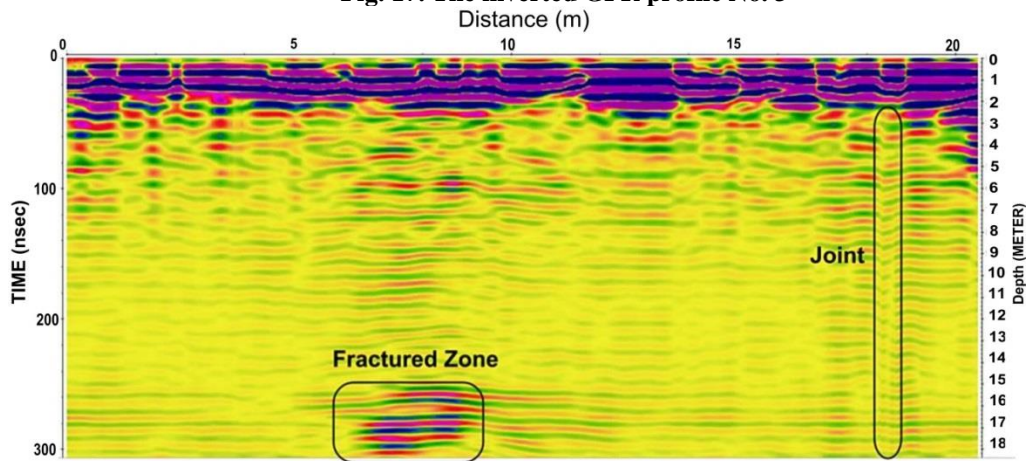
Fig. 18. The inverted GPR profile No. 4
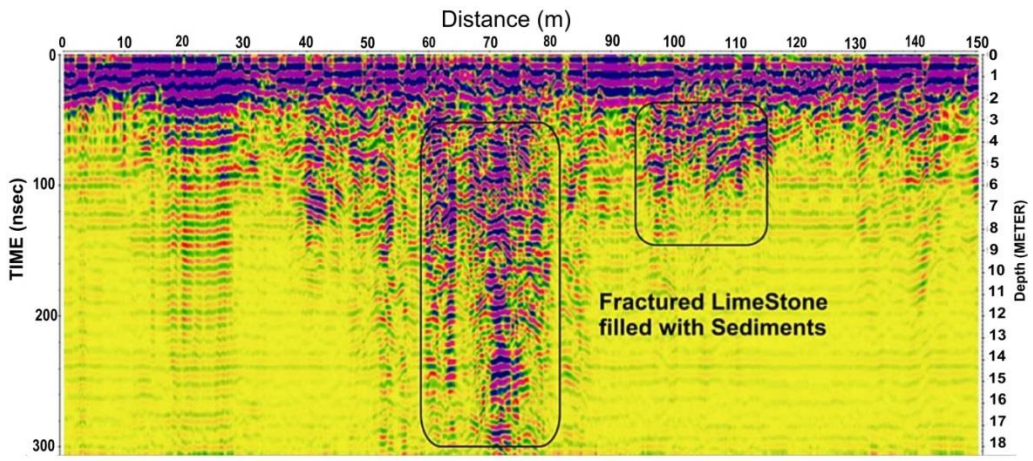
Fig. 19. The inverted GPR profile no. 5
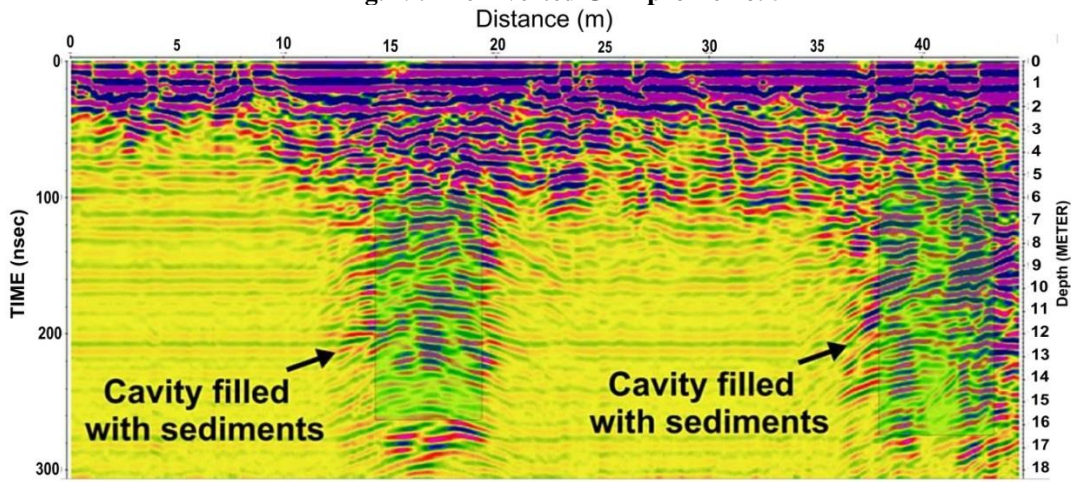
Fig. 20. The inverted GPR profile no. 6
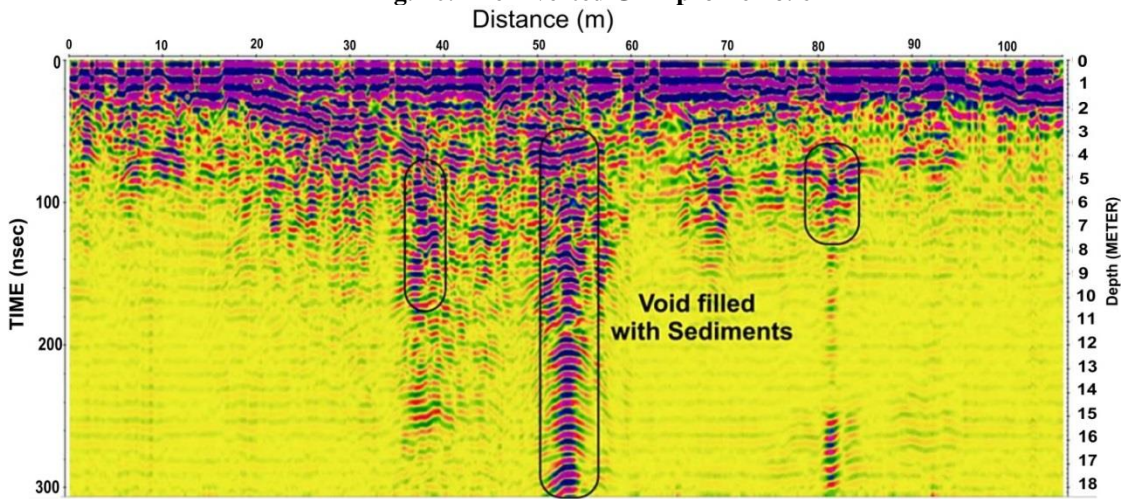
Fig. 21. The inverted GPR profile no. 7

Table 4: Locations of the cavities/voids and fracture-filled sediments.

Cavities / Voids / Fracture	Easting	Northing	Depth (m)	Dimensions (m)
Cavity filled with sediments	442670.00 m E	3254359.00 m N	5-18	7*13
Cavity filled with sediments	442702.00 m E	3254365.00 m N	6-18	6*12
Cavity filled with sediments	442684.00 m E	3254374.00 m N	6-18	5*12
Void filled with sediments	442658.00 m E	3254438.00 m N	4-18	3*14
Fracture filled with sediments	442693.00 m E	3254410.00 m N	4	5*13
Fracture filled with sediments	442677.00 m E	3254421.00 m N	4	5*13

Discussion

The primary aims of the current investigation are to identify the various underground voids and cavities, and to interpret the results in terms of the characteristics and materials of the foundation rock. The integrated geophysical methods are conducted to delineate the subsurface structures and fracture zones within 15 m of ground level. The integrated results obtained from the interpretation of both of the ERT and the SSR records conducted over the suspected site in the study area could be classified lithologically into three layers, which are the main geological units based on variation in resistivity and seismic velocities according to competence of bed with slight variation in thickness from one profile to another. The first zone is the top layer of weathered limestone, gravel shards, and fractured marl, which is distinguished by poor to somewhat good rock quality. The previous layer is overlaid by the second one, which has a lithology of fractured limestone of intermediate competent rock quality. The third zone is a bedrock layer because it contains the toughest layer of limestone and is distinguished by the high quality of competent rock. The geotechnical properties are estimated for the soil material at the project site based on the compressional-wave velocities (V_p), shear-wave velocities (V_S), and bulk densities to provide direct information about its material quality. These geotechnical parameters are vital for civil engineering and for evaluating the competence of the subsurface material (soil and/or rock) for construction purposes. The velocity range of the bedrock at the study site is about 1652 to 1720 m/sec for S-wave, which is refers to very compact and hard limestone. According to ASCE-7 code, the bed rock is classified as Hard Rock (Table 7).

Table 5: Example of Shear-wave (S-wave) velocity in different rock types, according to (ASCE 7: Minimum Design Loads for Buildings and Other Structures).

Site Class	Soil Profile	Shear Wave Velocity (m/sec) Shear Wave Velocity (m/s)
A	Hard Rock	Vs>1500
A	Hard Rock	Vs>1500
B	Rock	760<Vs $\leq$1500
B	Rock	760<Vs $\leq$1500
C	Very dense soil and soft rock	360<Vs$\leq$760
C		360<Vs$\leq$760
D	Stiff soil	180<Vs<360
D	Stiff soil	180<Vs<360
E	Soft soil	Vs<183
E	Soft soil	Vs<183

Based on the estimated geotechnical parameters from Vp and Vs and density, Poisson's ratio ranges between 0.251-0.273 for the first layer marked by a comparatively high Poisson's ratio indicating that the rocks are easily fractured and showing a fair to moderate level of competence, and the elastic modulus ranges from 442 MPa to 515.2 MPa and the shear (rigidity) modulus ranges from 176.6 MPa to 202.4 MPa and the bulk modulus ranges from 296.3 MPa to 377.8 MPa and its compressibility ranges between 26.47 X 10-4 to 33.74 X 10-4 MPa. This result will indicate that the first layer is weak and fissured and subjected to sinkholes buried with recent sediments. The Vp of the second layer increases the ranges from 1516 m/s to 1735 m/s leading to a decrease in Passion's ratio range from 0.218 to 0.23 indicating the rocks are harder to fracture than the overlaying layer. The elastic modulus ranges between 3903 MPa to 5192.5 MPa and the shear modulus is 1601.8 MPa to 2110.2 MPa and the bulk modulus ranges from 2309.9 MPa to 3209 MPa, and its compressibility ranges between 3.12 X 10-4 MPa to 4.33 X 10-4 MPa moderate values of elasticity are revealed by the elasticity moduli, which reflects that this layer is composed of consolidated layer of moderate elasticity after being subjected to the weathering process caused by water that flows during seasonal rainfall. The resultant values of elastic moduli of the third layer show that the layer is characterized by good competent rock quality according to Table (8) is characterized by low Poisson's ratio with Poisson's ratio value ranging between 0.131-0.148 indicating the rocks are harder to fracture than the first and second layer. The elastic modulus ranges between 13829 MPa to 14873.1 MPa and the rigidity modulus 6023.7 MPa to 6573.8 MPa and the bulk modulus ranges between 6546.8 MPa to 6722 MPa, and its compressibility ranges between 1.49 X 10-4 to 1.53 X 10-4 MPa. The values of the elastic, shear (rigidity), and bulk moduli are increased by increasing the velocities, resistivities, and densities.

Table 6: Classification of soil's competent according to Poisson's ratio, (Khalil, and Hanafy, 2008)

Soil description	Incompetent to Slightly competent	Fairly to moderately competent	Competent material	Very highly competent materials
Poisson's Ratio (δ)	0.41 – 0.49	0.27 – 0.35	0.16 – 0.25	0.03 – 0.12

Conclusion

Geophysical imaging of the buried rock discontinuities in the urban areas and new cities should not only overcome the suitability of site and determine the site characterization before construction but also can solve the future problems caused by land use and anthropogenic activities. Therefore, it is important to consider the multiplicity of geophysical and geotechnical techniques available in urban to study the problems of foundation soil and bedrock characterization, which threaten the construction of the area. In the present study, the combining use of different geophysical methods are employed to delineate the geological discontinuities and to map the geotechnical parameters and structural features that have a direct effect on foundation and urban planning in the study area. The integrated results of electrical resistivity, seismic refraction and ground penetrating radar surveys revealed that the suggested site consists of three subsurface layers alternated lateral and vertical due to the geological discontinuities. The first one is the surface layer of weathered limestone, fragments, and gravels, the second layer is composed of fractured limestone, and the third layer is composed of compacted and hard layer of limestone.

The ERT and velocity inverted sections indicate that the area exhibits more dense materials of high resistivities and velocities reflecting the high competent at shallow depths. A number of normal faults were delineated at different locations, while the limestone bedrock at shallow depths exhibits fractures and sinkholes that are filled with fine materials. This indicates that great care should be taken when designing the foundation system along the bedrock discontinuity and in the undeveloped parts of the Galala City. In prospective, the eastern part of the area, if water escapes into fracture zones along the mountain's edge, it might potentially cause problems with the soil engineering. The results of 2D resistivity and seismic refraction were well matched, demonstrating the suitability of these techniques for use in near-surface bedrock mapping, which can strengthen the case for borehole data and other physical mapping as well as complement it.

References

Abd El-Rahman, M., 1989, Evaluation of the kinetic elastic moduli of the surface materials and application to engineering geologic maps at Maba-Risabah area (Dhamar Province), Northern Yemen. Egypt. J. Geol, Vol, 33, Issue (1–2), pp. 229–250.

Araffa, S.A.S., Atya, M., Adel M.E. Mohamed, Mahmoud Gabala, Mohamed Abdel Zaher, Mamdouh, M. Soliman, Hany S. Mesbah, Usama Massoud, Hany M. Shaaban, 2014. Subsurface investigation on Quarter 27 of May15th city, Cairo, Egypt using electrical resistivity tomography and shallow seismic Refraction Techniques, NRIAG Journal of Astronomy and Geophysics, Vol 3, Issue 2, pp. 170-183. https://doi.org/10.1016/j.nrjag.2014.10.004

Attwa M, El Shinawi A., 2014, Geoelectrical and geotechnical investigations at tenth of Ramadan City, Egypt—a structure based (SB) model application. Near surface geoscience 2014-20th European meeting of environmental and engineering geophysics. https://doi.org/10.3997/2214-4609.20142007

B. Sjogren, 1984, Shallow Refraction Seismics, Chapman & Hall., vii, London, New York, pp. 270.

Baban Ezzadin N., Amin Abdulla K, Mohammed Sazan S., 2022, Seismic Refraction Tomography and Geotechnical Parameters to Assess the Chaqchaq Dam failure in NW Sulaimani City, Kurdistan Region, Iraq, Iraqi National Journal of Earth Science, Vol. 22, Issue 2, pp 121-139. https://doi.org/10.33899/earth.2022.135251.1027

Birch, F., 1966, Handbook of physical constants. Geol. Soc. Amer. Men. Vol.97, pp. 613.

Boudreault, J.P.; Dubé J.S.; Chouteau, M.; WiniarskiT. Hardy, É., 2010, Geophysical characterization of contaminated urban fills, Engineering Geology, vol. 116, pp. 196–206. https://doi.org/10.1016/j.enggeo.2010.09.002

Continental Oil Company (CONOCO), 1987. Stratigraphic Lexicon and Explanatory Notes to the Geologic map of Egypt 1: 500000. Edited by Maurice Hermina, Eberhard and franz K. list.

Eleraki, M., M. Gadallah, K. Gemail and M. Attwa, 2010. Application of resistivity method in environmental study of the appearance of soil water in the central part of Tenth of Ramadan City, Egypt. Quarterly. Journal of Engineering Geology and Hydrology, vol. 43, pp. 171–184. https://doi.org/10.1144/1470-9236/08-079

Farouk, S., 2015, Upper Cretaceous sequence stratigraphy of the GalalaPlateaux, western side of the Gulf of Suez, Egypt. Marine and Petroleum Geology, Vol. 60, pp.136-158. https://doi.org/10.1016/j.marpetgeo.2014.11.005

Gemail K.S., Shebl Salah, Attwa M., Soliman Shokry A., Azab Ahmed, Farag M.H., 2020, Geotechnical assessment of fractured limestone bedrock using DC resistivity method: a case study at New Minia City, Egypt, NRIAG Journal of Astronomy and Geophysics, vol. 9, no. 1, pp. 272- 279. https://doi.org/10.1080/20909977.2020.1734999

Khalil, M.H., Hanafy, S.M. 2008, Engineering applications of seismic refraction method: A field example at Wadi Wardan, Northeast Gulf of Suez, Sinai, Egypt‖, Journal of Applied Geophysics, Vol. 65, pp. 132- 141. https://doi.org/10.1016/j.jappgeo.2008.06.003

Leckebusch, J., 2003, Ground- penetrating Radar: Modern Three-dimensional Prospection Method. Archaeo. Prospect, Vol. 10, pp. 213–240. https://doi.org/10.1002/arp.211

Mohamed H. Khalil, Sherif M. Hanafy, 2008, Engineering applications of seismic refraction method: A field example at Wadi Wardan, Northeast Gulf of Suez, Sinai, Egypt, Journal of Applied Geophysics, Vol. 65, pp. 132-141. https://doi.org/10.1016/j.jappgeo.2008.06.003

Loke, M. H. and Barker, R. D., 1992, Rapid least-squares inversion of apparent resistivity pseudosection by a quasi-Newton method. Geophys, Prospect., Vol. 44, pp. 131-152, https://doi.org/10.1111/j.1365-2478.1996.tb00142.x

Loke, M.H, 2020, Tutorial: 2-D and 3-D electrical imaging surveys. Penang, UniversitiSains Malaysia, unpublished course notes. World Wide Web Address: www. Geoelectrical com.

Othman, A.A.A., 2005, Construed geotechnical characteristics of foundation beds by seismic measurements. J. Geophys. Eng. Vol. 2, pp. 126–138. https://doi.org/10.1088/1742-2132/2/2/007

Parry R H G, 1977, Estimating bearing capacity of sand from SPT values JGED ASCE Vol. 103, pp. 1014–1043.

Perrone A., Iannuzzi A. et al., 2004, High-resolution electrical imaging of the Varco d'Izzo earthflow (southern Italy). J Appl Geophys, vol. 56, Issue 1, pp. 17–29. https://doi.org/10.1016/j.jappgeo.2004.03.004

Sasaki, Y., 1996, Resolution of resistivity tomography inferred from numerical simulation‖, Geophysical Prospecting, Vol. 40, pp. 453-464. https://doi.org/10.1111/j.1365-2478.1992.tb00536.x

Shebl S, Gemail KS, Attwa M, Soliman SA, Azab AA, Farag MH, 2019, Utilizing shallow seismic refraction in defining the geotechnical properties of the foundation materials: a case study at New Minia City, Nile Valley, Egypt. J Pet. vol. 28, pp. 145–154. https://doi.org/10.1016/j.ejpe.2018.12.006

Shokry A. Soliman, Hossam M. El-Sayed, T.F. Shazly, and Abdellatif Younis, 2020, Combined Application of Electrical Resistivity and GPR Techniques for Water Seepage Detection at New Cairo City, Egypt.Current Science International, Vol. 9, pp. 630-640.

Shokry A. Soliman, Salah Shebl, Ahmed El Khafif, T.F. Shazly, M.H. Farag, 2021, Preliminary assessment of the Soil Foundation Characteristics Utilizing the 2D Resistivity Imaging and Down-Hole Seismic Refraction Techniques: A Case Study in Tenth of Ramadan City, Egypt.Iraqi   Journal   of   Science,   Vol.   62,   pp.   3587-3600, https://doi.org/10.24996/ijs.2021.62.10.17

Silva, C.P.L. 2011, Cartografia Geotécnica Tridimensional do Setor Noroeste de Brasília. Publicação G.TD 072/2011. Universidade de Brasília – UnB, Brasília, 299p. Tese (Doutorado), Departamento de Engenharia Civil Ambiental,

Stumpel, M., Kahler, S., Meissner, R., Nikereit, B., 1984, The use of seismic shear waves and compressional waves for lithological problems of shallow sediments. Geophys. Prospect. Vol. 32, pp. 662–675, https://doi.org/10.1111/j.1365-2478.1984.tb01712.x

Thomsen, L., 1986. Weak Elastic Anisotropy. Geophysics, Vol. 51, pp. 1954-1966. https://doi.org/10.1190/1.1442051